ACS Catalysis

pubs.acs.org/acscatalysis
Research Article

Metal–Oxide Interface Sites Created Using Atomic Layer Deposition and Tested for CO Oxidation

Wang Ke, Ilkeun Lee, and Francisco Zaera*

Cite This: ACS Catal. 2025, 15, 12281–12292
Read Online

ACCESS | Metrics & More | Article Recommendations | Supporting Information

ABSTRACT: The performance of catalysts made out of Pt supported on TiO_2 thin films grown on SBA-15 (a silica mesoporous material) by atomic layer deposition (ALD) was characterized systematically by combining in situ infrared absorption spectroscopy (IR) with other techniques including electron microscopy and adsorption–desorption isothermal measurements. The titania films in the resulting high-surface-area catalysts were evenly distributed throughout the inner surface of the SBA-15 mesopores, and their thickness could be controlled at a submonolayer level, with 3 to 4 TiO_2 ALD cycles needed for the complete coverage of the silica sites. The titania films could be deposited either before or after adding the metal (Pt), which was dispersed in the form of small nanoparticles (NPs) approximately 4–6 nm in diameter, in order to exert some control on the density and nature of the Pt/TiO_2 interface sites. One important lesson deriving from this work is that such an order of deposition leads to significantly different catalysts in spite of the fact that most of their structural properties are similar. If the Pt is deposited on the titania films, the resulting metal NPs are slightly smaller than those grown on silica and display CO adsorption sites with lower surface Pt coordination numbers. On the other hand, when TiO_2 is deposited on the Pt/SBA-15 starting material, some titania grows on the metal and partially blocks its surface while also creating new interface sites where CO binds more weakly and displays lower C–O stretching frequencies. In terms of catalytic performance, the results from in situ IR CO site titration and kinetic measurements combined suggest a mechanism where CO first adsorbs on Pt atop sites and then migrates to Pt/TiO_2 interface sites, where oxidation takes place. Both types of sites appear to be similar in all the catalysts tested, but catalytic performance could be optimized by tuning their surface densities. Maximum catalytic activity was obtained when the TiO_2 films were deposited first and with TiO_2 coverages of at least half a monolayer, that is, after at least 2 ALD cycles.

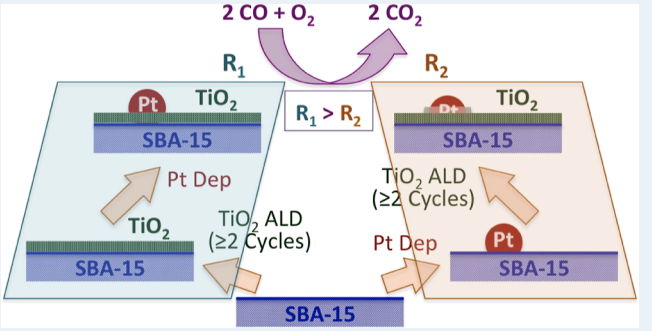

KEYWORDS: *oxidation catalysis, metal–oxide interface, titania, platinum, atomic layer deposition, in situ infrared absorption spectroscopy, carbon monoxide*

1. INTRODUCTION

Many oxidation reactions can be promoted by using reducible oxides as catalysts. They usually follow the so-called Mars–van Krevelen (MvK) mechanism, by which the reactant is oxidized by oxygen atoms from the oxide lattice and the ensuing vacancies are replenished with oxygen from the gas phase.[1−3] Such oxidation catalysis, in particular oxygen incorporation into the reactant, can be aided by the addition of a metal in nanoparticle (NP) form, commonly a transition metal. Much has been learned in this area from studies with gold,[4−9] but other metals have been used as well, including platinum.[10−14] The reaction between surface oxygen atoms and the adsorbed reactant is generally believed to take place at the interface between the metal and the oxide,[15−17] but the detailed characterization of that step, of both the structure of the active sites and the reaction intermediates, has been challenging. Not only are there only a limited number of spectroscopies that can be used in situ to interrogate the surface during reaction, but it is also difficult to control the structural details of the catalyst during its synthesis.

Here, we attempt to provide further insights into these oxidation reactions by using catalysts where Pt NPs were dispersed on titanium oxide (TiO_2) deposited as a thin film on SBA-15, a silica mesoporous material with a high surface area and well-defined one-dimensional pores of approximately 6–7 nm in diameter arranged in a honeycomb pattern.[23−25] The thickness of the film was tuned with submonolayer accuracy by using atomic layer deposition (ALD), a technique where a surface chemical reaction yielding a solid product is split into

Received: May 9, 2025
Revised: June 27, 2025
Accepted: June 30, 2025
Published: July 7, 2025

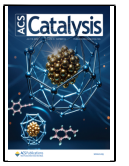

https://doi.org/10.1021/acscatal.5c03164
ACS Catal. 2025, 15, 12281–12292

two self-limiting and complementary steps to grow films homogeneously and conformally.[18−22] Infrared absorption spectroscopy (IR) was used in situ to characterize the catalytic surface sites as well as to follow the kinetics of our probe reaction, the oxidation of carbon monoxide (CO) with O_2. Our approach afforded the creation of titania-based high-surface-area catalysts, something difficult to achieve with bulk titania, and to systematically control both the titania film thickness and the time at which it is added to the catalyst, either before or after the deposition of the Pt NPs. By tuning those parameters, it was possible to optimize the catalytic performance and to acquire some knowledge of the factors that contribute to the catalytic activity.

2. EXPERIMENTAL SECTION

A total of nine catalysts were synthesized by combining the deposition of TiO_2 thin films via ALD with the growth of Pt NPs via wet impregnation on commercial SBA-15 (Sigma-Aldrich, research purity): two sets of four catalysts each, denoted as Pt/(x-ALD-TiO_2)/SBA-15 and (x-ALD-TiO_2)/Pt/SBA-15, were made by performing x = 1 to 4 ALD cycles either before or after Pt NP deposition (respectively), and a ninth Pt/SBA-15 catalyst was prepared for reference (and as the starting material upon which the TiO_2 films were grown by ALD in the (x-ALD-TiO_2)/Pt/SBA-15 cases). Samples with TiO_2 films but without Pt, (x-ALD-TiO_2)/SBA-15, were also synthesized for reference.

The ALD of the TiO_2 films was carried out in a homemade batch reactor already described elsewhere.[26−28] The main chamber of the reactor is based on a six-way stainless steel cross with 2.75 in. Conflat flanges, and is heated to 375 K during the ALD processes (to avoid condensation of the gases on the inner walls) by using a set of heating tapes wrapped around its outside. A sample tray 3 × 2 × 0.5 cm^3 in size is attached to electrical feedthroughs by Ni wires to allow for resistive heating to 375 K during the depositions, as monitored using a K-type thermocouple spotwelded to the backside of the tray and set independently from that of the chamber by using a separate controller. The tray is filled with the powder samples to a depth of approximately 1 mm and covered with a tightly fitted lid made out of a stainless steel wire mesh to hold them in place and prevent them from being blown away during pumping and purging.

Two independent gas lines are attached to two of the flanges bolted to the reaction chamber for the delivery of the precursor/water and purging gases, respectively. The chemicals are fed into the system directly as gases, taking advantage of their high vapor pressures (after mild heating when needed). The reactor is evacuated using a mechanical pump connected to the six-way cross via a 1.5 in. right-angle valve and typically reaches ultimate pressures of around or below 5 mTorr, as measured by a thermocouple gauge. In a typical ALD cycle, the SBA-15 powder (or a Pt/SBA-15 catalyst if the Pt was deposited first) was exposed alternately to vapors of tetrakis-(dimethylamido)Ti(IV) (TDMAT, Aldrich-Sigma, 99.999% purity in a trace metals basis; heated to 315 K during the ALD processes for vapor delivery) and deionized (DI) water interspersed with purging exposures to N_2 (Airgas), all at 375 K, typically using the following cycle times: TDMAT/N_2/H_2O/N_2 = 20 min:50 min:2 min:50 min. This procedure was shown previously to deposit TiO_2 films evenly throughout the full length of the SBA-15 nanopores.[26]

The catalysts where the metal (Pt) was deposited first were synthesized by a colloidal method: 2.59 mL of a 0.006 mol/L $H_2PtCl_6{\cdot}6H_2O$ (Strem chemicals, 99.9%) aqueous solution, 2.4 mL of deionized (DI) water, 45 mL of ethanol (Koptec, 200 proof), 0.060 g of polyvinylpyrrolidone (PVP, Sigma-Aldrich, average molecular weight 10,000), and 0.3 g of SBA-15 were mixed together, sonicated for 30 min, and stirred using a magnetic stirrer for 1 h. The suspension was transferred to a 2-neck flask with an attached condenser and refluxed at 360 K (measured using a thermocouple inserted in the reaction volume) for 3 h while stirring. The powder was centrifuged, dried, calcined under O_2 (99.5%, Airgas) at 775 K for 24 h, and reduced under H_2 (99.9%, Airgas) at 575 K for 2 h to remove the surfactant (PVP). The Pt deposition on the supports previously covered with titania films (by ALD, the (x-ALD-TiO_2)/SBA-15 solids) was done via precipitation: 0.86 mL of a 0.006 mol/L $H_2PtCl_6{\cdot}6H_2O$ aqueous solution, 20 mL of DI water, and 100 mg of the (x-ALD-TiO_2)/SBA-15 were mixed together and sonicated for 30 min, after which the solvent was removed via rotary evaporation at 330 K for 3 h. After the catalysts were fully dried, they were reduced under H_2 at 625 K for 3 h.

The scanning transmission electron microscopy (STEM) images were acquired by using a FEI Titan Themis 300 instrument equipped with a Bruker Quantax detector for energy-dispersive X-ray spectroscopy (EDX) imaging. The mesopores in the SBA-15-based catalysts were characterized using isothermal N_2 adsorption−desorption data acquired with a NOVA@2000e gas sorption system and analyzed using the Nova Win software. The TiO_2 and Au loadings were measured by using a PerkinElmer Optima 7300DV inductively coupled plasma atomic emission spectroscopy (ICP−AES) apparatus.

The transmission infrared spectroscopy (IR) characterization and in situ kinetic experiments were performed using a Bruker Tensor 27 Fourier transform infrared (FTIR) spectrometer equipped with a mercury−cadmium−telluride (MCT) detector, together with a homemade quartz cell with NaCl windows described in more detailed elsewhere.[29,30] Self-supporting disks approximately 13 mm in diameter were made with ∼10 mg of each catalyst and placed in the center of the cell, degassed at 425 K for 2 h under vacuum, and sequentially oxidized and reduced three times at 625 K under 200 Torr of O_2 and H_2, respectively, for 1 h each. For the carbon monoxide (CO, 99.5%, Matheson Tri-Gas) characterization experiments, each catalyst was cooled down to below 125 K and exposed to 20 Torr of CO for 10 min, after which the cell was evacuated. Transmission IR spectra were then acquired at 10 K intervals while slowly heating up the sample until reaching a temperature of 625 K. It should be indicated that at cryogenic temperatures, water condensation was found to interfere with the adsorption of CO on the Pt metal surface. However, this could be easily addressed by focusing on the data recorded above approximately 225 K, at which point all adsorbed water has already desorbed and been pumped away. All of the spectra were recorded at a resolution of 4 cm^{-1} and referenced to background traces recorded under similar conditions before CO adsorption.

For the kinetic experiments, the cell was filled with a premixed 100 Torr CO + 100 Torr O_2 gas mixture, after which the temperature was increased to 525 K, and IR spectra were taken periodically as a function of time for 3 h. The partial pressures of CO and CO_2 were determined by using the integrated intensities of the appropriate IR bands (the 2050−

https://doi.org/10.1021/acscatal.5c03164
ACS Catal. 2025, 15, 12281−12292

2240 and 2240−2400 cm^{-1} regions, respectively) after calibration of the signal intensities, and converted to moles using the ideal gas equation and the measured value of the volume of the IR cell. From there, turnover numbers (TONs) were estimated after calculating the total number of Pt atoms exposed using the metal loads and NP average sizes (assuming spherical particles). Turnover frequencies (TOFs) were calculated by numerical derivation of the TON-versus-time data and are expressed in units of s^{-1}.

3. RESULTS

The physical properties of the catalysts were first characterized using a combination of techniques. The geometrical details of the mesopores of the solid support after the ALD of the TiO_2 films were extracted from isothermal N_2 adsorption−desorption data. As previously reported for the deposition on both pure SBA-15[26,27] and on catalysts made out of Au NPs dispersed on the same silica support,[31,32] the TiO_2 films were found to grow uniformly throughout the length of the mesopores at a rate of approximately 1.2 Å/cycle. The relevant data are provided in Figures 1 and S1 (Supporting Information): the narrowness of the pore size distributions attests to the homogeneity of the film (Figure S1), and the approximately linear decrease in the average pore diameter with the number of ALD cycles used provides the information from which the film growth rates could be extracted (Figure 1, left panel). The decreases in the surface area (Figure 1, center panel) and total pore volume (Figure 1, right) with increasing number of ALD cycles are consistent with the reductions in pore diameter reported in the left panel of Figure 1. Critically, it can be seen from these results that the dimensions of the pores in these catalysts are the same (for the same number of ALD cycles, x), within the errors of the experiments, in the three families of catalysts, indicating that the deposition of the Pt NPs either before or after TiO_2 film growth does not affect the ALD process in any appreciable way.

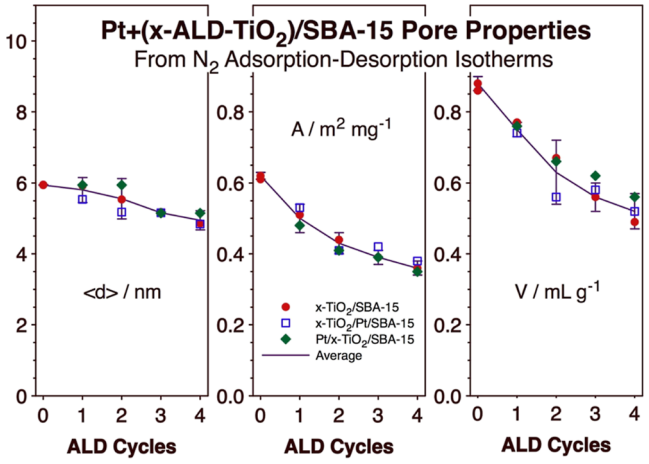

Figure 1. Pore average diameters ($\langle d \rangle$, in nm; left panel), surface areas (A, in m^2/mg; center), and total volumes (V, in mL/g; right), all plotted as a function of the number of TiO_2 ALD cycles used. Data are provided for the three sets of catalysts, (x-ALD-TiO_2)/SBA-15 (red-filled circles), (x-ALD-TiO_2)/Pt/SBA-15 (blue open squares), and Pt/(x-ALD-TiO_2)/SBA-15 (green-filled diamonds). The error bars correspond to the standard deviations of the results from three sets of measurements made in each case using three different batches of catalysts.

The TiO_2 and Pt content of our catalysts were estimated by ICP−AES and are reported in Figure 2 in terms of weight %,

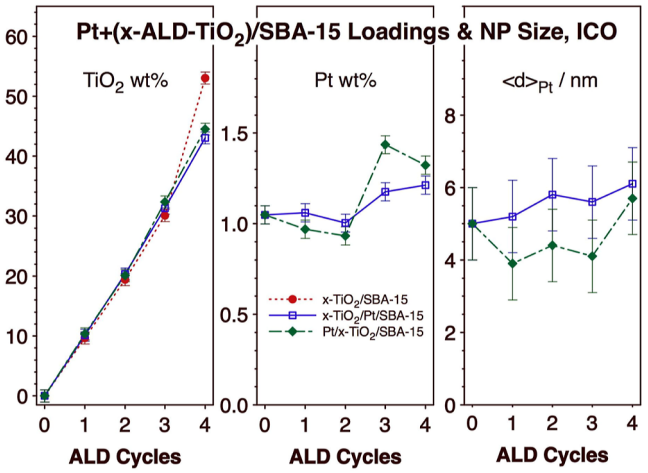

Figure 2. TiO_2 (left panel) and Pt (center) weight percentages (wt %), measured by ICP−AES, and average Pt NP diameters ($\langle d \rangle_{Pt}$, in nm; right), estimated from STEM images (Figure S2, Supporting Information), for the three sets of catalysts, (x-ALD-TiO_2)/SBA-15 (red-filled circles and dashed lines), (x-ALD-TiO_2)/Pt/SBA-15 (blue open squares and solid lines), and Pt/(x-ALD-TiO_2)/SBA-15 (green-filled diamonds and dash-dot lines), all as a function of the number of ALD cycles used (x). The error bars in the left and center panels correspond to the standard deviations of results from three sets of measurements made using three different batches of catalysts, whereas those in the right panel correspond to the standard deviations of the size values of 100 Pt NPs.

referenced to the mass of the initial SBA-15 substrate (left and center panels, respectively). The mass of TiO_2 was seen to grow in an approximately linear fashion with the number of ALD cycles (x), at the same rate in all three types of catalysts; again, the addition of Pt NPs either before or after the TiO_2 deposition does not appear to significantly alter the physical nature of the latter. It should be indicated, however, that previous studies highlighted the fact that the density of the new oxide films is initially much lower than those of crystalline titania and only approaches the latter values after multiple (≥10) ALD cycles;[27] the same behavior was observed in the present case. In terms of the Pt content of the catalysts, it was close to the targeted value of 1 wt % in all cases (Figure 2, center), except for an apparent increase after several TiO_2 ALD cycles on the samples where the Pt was deposited afterward: possibly, the nucleation and growth of the Pt NPs on the TiO_2 films is different than on the underlying silica substrate. The Pt NP average sizes, extracted from the size distributions estimated from STEM images (Figure S2, Supporting Information) and reported in the right panel of Figure 2, also indicate a slight difference between the two sets of catalysts, with the NPs grown on the TiO_2 films being, in general, somewhat smaller than those deposited on the naked SBA-15. Nevertheless, the differences are not large and are likely not significant in relation to our later evaluation of the activity of the catalysts.

A general assessment of the quality of the catalysts was further pursued by acquiring STEM and EDX images of representative samples, as illustrated in Figure 3. The images indicate good dispersions for both the TiO_2 films and the Pt NPs all throughout the inside of the pores. The former is

https://doi.org/10.1021/acscatal.5c03164
ACS Catal. 2025, 15, 12281−12292

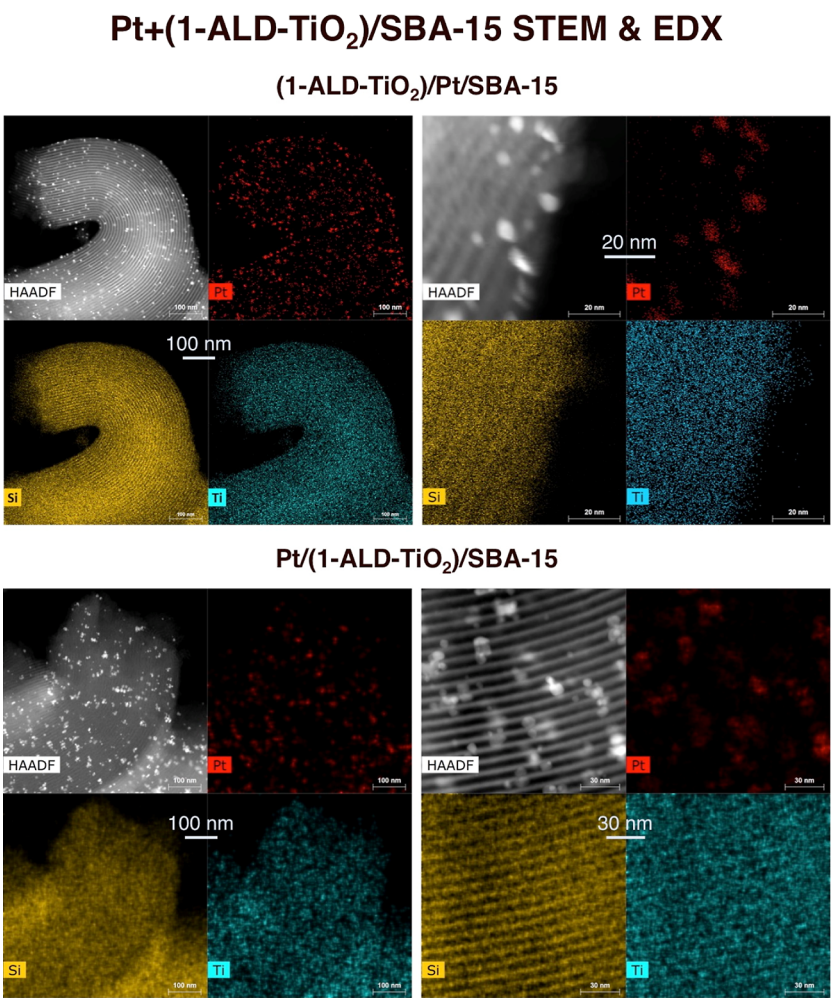

Figure 3. STEM (top left in each image set) and Pt (top right), Si (bottom left), and Ti (bottom right) EDX images of two representative catalysts, (1-ALD-TiO_2)/Pt/SBA-15 (top set) and Pt/(1-ALD-TiO_2)/SBA-15 (bottom), imaged at two different scales, approximately 600 nm (100 nm scale bar, left sets) and either 80 (20 nm scale bar, top right) or 150 (30 nm scale bar, bottom right) nm in total size. With both samples, the Ti and Pt EDX images indicate full dispersion of both elements all throughout the length of the pores.

particularly encouraging, because the design of the ALD process requires avoiding mass transport limitations during exposure to the chemicals involved, and in the case of SBA-15 the conditions are quite restrictive, given that the pores are approximately 6−7 nm in diameter but hundreds of nanometers in length.[26] Again, high-quality catalysts were obtained regardless of the order of the Pt NP deposition and TiO_2 ALD.

The adsorption sites of our catalysts were characterized by using IR absorption spectroscopy in combination with carbon monoxide as the probe molecule. Each catalyst was saturated with CO, after which IR spectra were then taken under a vacuum as a function of temperature. At cryogenic temperatures, CO adsorption was detected on both the metal and the oxide support; Figure 4 reports the corresponding spectra recorded at 125 K. A transition is observed in all (x-ALD-TiO_2)/SBA-15, Pt/(x-ALD-TiO_2)/SBA-15, and (x-ALD-TiO_2)/Pt/SBA-15 catalysts with increasing TiO_2 coverage, that is, as the number of TiO_2 ALD cycles is increased, a trend similar to what we have already reported for (x-ALD-TiO_2)/SBA-15,[27] Au/(x-ALD-TiO_2)/SBA-15,[32] and (x-ALD-TiO_2)/Au/SBA-15[28,32] catalysts. The spectrum for CO adsorbed on pure SBA-15 (Figure 4, left panel, bottom—green—trace) shows a primary peak at 2155 cm^{-1} accompanied by a smaller feature at 2137 cm^{-1}, as reported by us previously;[28] these peaks have been assigned to CO bonded to the silanol groups of silica.[33] The addition of Pt to the silica support suppresses those peaks at the expense of the growth of a single, sharp, and intense peak at 2102 cm^{-1} (Figure 4, center and right panels, bottom—green—traces), typical of adsorption on Pt atop sites.[34−36]

The IR peaks due to CO adsorption on the silica surface decrease gradually as thicker TiO_2 films are deposited, that is, as the number of TiO_2 ALD cycles are increased. As reported in the past, this transition requires multiple ALD cycles but is complete by 4 cycles, at which point the surface is fully covered with a titania film.[27] Curiously, though, the IR spectra of CO adsorbed on the newly deposited titania are different depending on the film-growth protocol. If the Pt NPs are added to the SBA-15 surface prior to the TiO_2 ALD, that is, with the (x-ALD-TiO_2)/Pt/SBA-15 catalysts, only one major peak is seen around 2189 cm^{-1} (Figure 4, right panel); this feature has been reported to correspond to adsorption on Lewis-acid titanium ion surface sites in both crystalline (rutile)[37] and amorphous[38−40] surfaces, on fully coordinated Ti sites (Ti_{5C}). On the other hand, if the titania films are grown on pure SBA-15, clear additional peaks are detected at 2159 and 2138 cm^{-1}; this is the case for both sets of samples with (Pt/(x-ALD-TiO_2)/SBA-15; Figure 4, center panel) and

https://doi.org/10.1021/acscatal.5c03164
ACS Catal. 2025, 15, 12281−12292

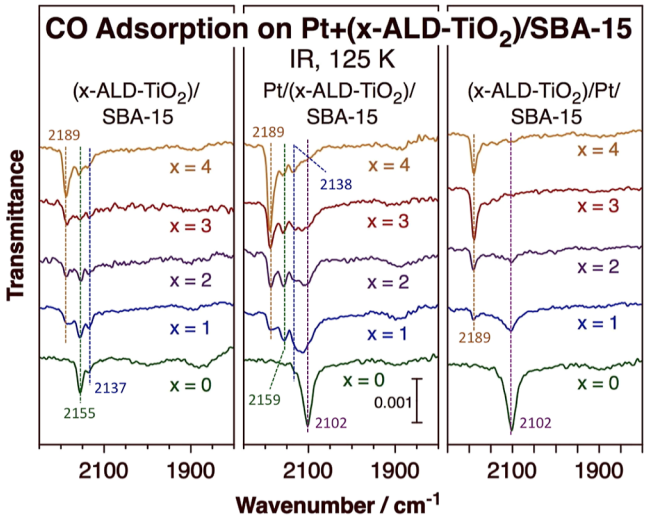

Figure 4. IR spectra for CO adsorbed on the (x-ALD-TiO_2)/SBA-15 (left panel), Pt/(x-ALD-TiO_2)/SBA-15 (center), and (x-ALD-TiO_2)/Pt/SBA-15 (right) catalysts, for x (number of TiO_2 ALD cycles) = 0 to 4. The data were obtained under vacuum after saturating the catalyst with CO at 125 K (exposing them to 20 Torr CO for 10 min) and pumping the gas away.

without ((x-ALD-TiO_2)/SBA-15; Figure 4, left) added Pt NPs. Literature reports have associated these IR features to CO adsorbed on oxygen sites with the molecular axis oriented either perpendicular or parallel to the surface plane (respectively),[41] but they could alternatively, and perhaps more likely, reflect an incomplete blocking of silica sites by the titania film. Adsorption on those sites appears to be inhibited in the (x-ALD-TiO_2)/Pt/SBA-15 catalysts, suggesting more efficient site blocking by the titania film in that case, possibly because the Pt NPs may catalyze a better dispersion of the growing TiO_2 film during ALD. It should also be pointed out that no indication of the formation of unsaturated Ti_{4C} sites was seen with any of the samples reported here. Those are typically seen at higher frequencies and were indeed observed in the equivalent gold-based catalysts.[32]

The CO IR titration experiments also provided new insights into the nature of the adsorption sites on the Pt surfaces. The relevant features became evident after warming the samples, as illustrated in the set of spectra reported versus temperature (from 275 to 415 K) for all of our catalysts in Figure S3 (Supporting Information). A selection of those traces is provided in Figure 5. A number of absorption features are seen in the 2000−2100 cm^{-1} frequency range, all associated with CO adsorbed on Pt surfaces, as the CO bonded to the oxides (SiO_2 and TiO_2) desorbs at much lower temperatures. The behavior is complex, as several peaks are detected, though, in sequences that are quite different depending on which of the two materials, Pt or TiO_2, was deposited first during the fabrication of the catalysts. With the Pt/SBA-15 catalyst, without any TiO_2 added, the peak initially seen at 2102 cm^{-1} red-shifts slightly, to 2093 cm^{-1} at 225 K, 2090 cm^{-1} at 275 K, and 2088 cm^{-1} at 285 K, as some CO desorbs and its coverage on the surface (and the intensity of the IR peak) decreases (Figure 5, bottom, green traces in both sets of panels, x = 0); this is a well-known trend due to changes in dipole−dipole interactions with coverages.[42] CO desorption from this catalyst is virtually complete by 325 K.

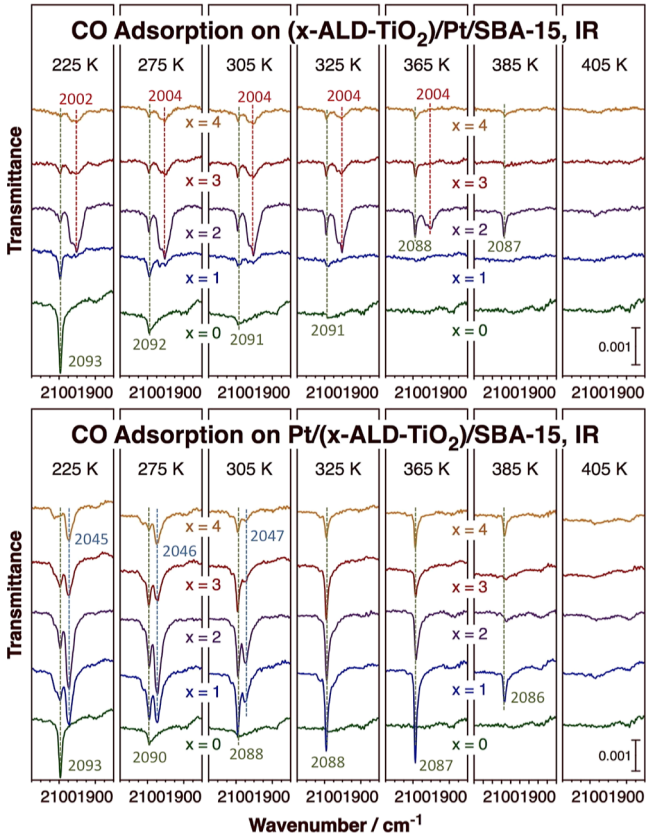

Figure 5. IR spectra for CO adsorbed on the (x-ALD-TiO_2)/Pt/SBA-15 (top row) and Pt/(x-ALD-TiO_2)/SBA-15 (bottom) catalysts saturated with CO (20 Torr CO exposure for 10 min), for x (number of TiO_2 ALD cycles) = 0 to 4. The data were obtained at the indicated selected temperatures as the samples were slowly heated in vacuum from an initial temperature of 125 K.

As TiO_2 is added to this Pt/SBA-15 catalyst, new features develop in the IR spectra due to CO adsorbed on the metal sites. The changes are barely detectable after only one TiO_2 ALD cycle (Figure 5, top row, second from bottom, blue traces, x = 1) but become dominant for x = 2 (middle, purple, traces), after which they decrease in intensity (together with the ∼2090 cm^{-1} original feature). Three additional overlapping peaks (in addition to the ∼2090 cm^{-1} feature) are seen in the IR spectra of these samples, the main one at 2002 cm^{-1} surrounded by shoulders at both ends, at 1982 and 2032 cm^{-1}. It is well known that the C−O stretching frequencies of CO adsorbed on Pt surfaces vary considerably with both surface coverage and the coordination of the Pt adsorption site,[35] but these values are well outside the range that could be justified this way. Instead, they are likely to reflect CO adsorption on Pt sites modified by TiO_2, possibly by a thin layer grown on top of the metal NPs akin to those associated with strong metal−support interactions (SMSIs).[43−47] Interestingly, the new IR features appear at lower frequencies than those for CO on regular Pt sites, implying more extensive back-donation from the Pt d orbitals to the π^* antibonding orbital of CO and/or a more negatively charged Pt atom.[48] This is the opposite of what has been reported for Au/TiO_2 catalysts, where typically the metal in the new interface sites is partially cationic.[32,49,50] As mentioned above, the coverage of the new Pt/TiO_2 interface sites is optimized after 2 TiO_2 ALD cycles, at which point about 50% of the initial silica surface is still

https://doi.org/10.1021/acscatal.5c03164
ACS Catal. 2025, 15, 12281−12292

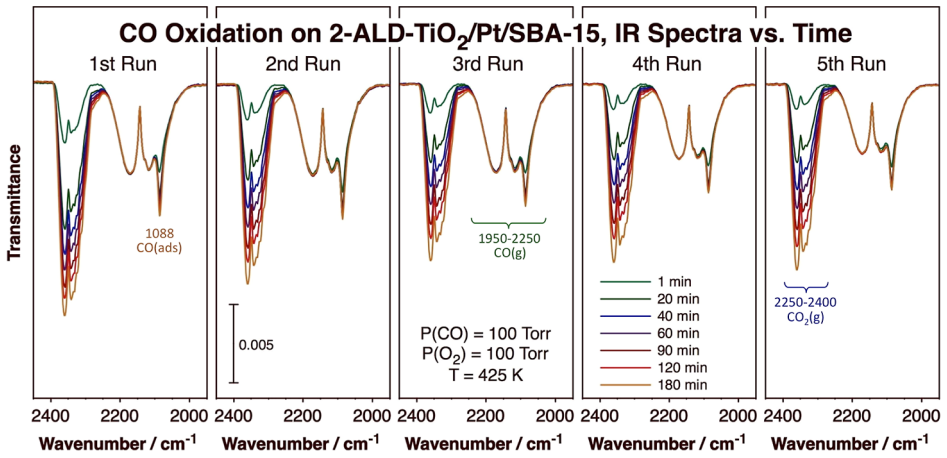

Figure 6. In situ IR spectra versus reaction time recorded during the conversion of 100 Torr CO + 100 Torr O_2 gas mixtures at 425 K promoted by the (2-ALD-TiO_2)/Pt/SBA-15 catalyst. Five sets of kinetics were obtained sequentially, the results of which are shown in the five panels presented here. In each panel, shown are the traces recorded after 1, 20, 40, 60, 90, 120, and 180 min of reaction, with colors transitioning from green to blue, red, and finally orange as the reaction time increases.

exposed (Figure 4);[27,28] further addition of TiO_2 blocks all sites, and after 4 TiO_2 ALD cycles, which deposit approximately one full monolayer, very few Pt adsorption sites remain exposed (Figure 5, top row). Another critical observation deriving from these data is that CO desorption from the surface obtained after adding TiO_2 to the Pt/SBA-15 catalyst requires much higher temperatures than from the substrate without the titania film: removal of CO from the Pt/TiO_2 interface sites in the former case requires heating to 385 K, and the CO adsorbed on the original atop sites, namely, the one associated with the ~2100 cm^{-1} IR peak, remains bonded to Pt to even higher temperatures, up to 405 K.

If the TiO_2 films are grown on the SBA-15 support prior to the addition of the Pt NPs, that is, with the Pt/(x-ALD-TiO_2)/SBA-15 catalysts, a very different behavior is observed for adsorbed CO, as shown in the bottom set of panels in Figure 5. Only one extra peak is observed in the IR traces, around 2045 cm^{-1}, upon addition of TiO_2 to the Pt/SBA-15-based catalysts. This feature appears to develop at the expense of the original atop adsorption site as the TiO_2 film is made thicker, until reaching an optimum coverage for x = 2 (2 TiO_2 ALD cycles, Figure 5, bottom row). The new frequency is again lower than that for the unmodified Pt/SBA-15 catalyst, but the shift in this case is not as large and it is possibly due to structural changes in the Pt NPs because of them having been grown on TiO_2 rather than on SiO_2 substrates. It has been reported that CO adsorption on small nanoparticles, which typically contain more low-coordination sites, yields lower C−O stretching frequencies.[51−54] This suggests that the Pt NPs grow in a more irregular form on titania than on the underlying silica support, a hypothesis consistent with the smaller Pt NP sizes seen by STEM in those cases (Figure 2). Counterintuitively, however, the CO adsorbed on the low-coordination sites, that is, the one associated with the IR peak around 2045 cm^{-1}, desorbs first and is gone by 325 K; the CO atop basal-plane Pt atoms, reflected by the 2090 cm^{-1} feature, remains on the surface up to approximately 405 K. Clearly, the addition of titania to the silica surface prior to the Pt NP deposition affects the energetics of adsorption of those sites as well.

The activity of our catalysts toward the oxidation of carbon monoxide with molecular oxygen was tested next using IR in situ as a function of the extent of the reaction. Either five (with the (x-ALD-TiO_2)/Pt/SBA-15 catalysts) or two (with the Pt/(x-ALD-TiO_2)/SBA-15 samples) consecutive runs for the conversion of 100 Torr CO + 100 Torr O_2 gas mixtures at 425 K, each for 3 h, were carried out while acquiring IR spectra in transmission mode. For this, the spent reaction mixture was pumped out and a fresh gas mixture was added to the reactor without any catalyst treatment in between. All of the spectral data from these studies are reported in Figures S4 and S5 (Supporting Information), and an example, for the case of the (2-ALD-TiO_2)/Pt/SBA-15 catalyst, is provided in Figure 6. Three regions are easily identified in these traces: (1) a set of multiple peaks in the 2250−2400 cm^{-1} region due to the gas-phase carbon dioxide being produced by the oxidation of CO; (2) a broad "m"-shaped feature between 1950 and 2250 cm^{-1} corresponding to the gas-phase CO in the reaction mixture; and (3) a sharp peak at about 2088 cm^{-1} associated with CO adsorbed on the Pt surface during reaction. A few clear observations can be highlighted from these data: (1) the CO_2 IR peaks clearly grow with time, a fact that affords a method to follow the kinetics of the CO oxidation; (2) the intensity of the IR absorption due to gas-phase CO decreases with time but only slightly: this decrease was used to corroborate the kinetics estimated using the CO_2 IR region but yielded much noisier results (the total CO consumption by the end of the 3 h reactions was approximately 1−2 Torr); and (3) the intensity of the adsorbed CO IR peak provides a direct measurement of the available Pt sites.

First, we discuss the latter point, the fraction of Pt sites available for catalysis during the CO oxidation reaction. The area of the 2088 cm^{-1} peak was calculated as a function of time for all runs with all of our catalysts, and the averages from all runs, normalized to the maximum CO coverage seen under reaction conditions for the Pt/SBA-15 catalyst, are plotted in Figure 7 (the error bars are the standard deviations of the individual measurements). It is seen there that a steady-state CO coverage is reached in each reaction only after tens of minutes into the catalytic runs (Figure 7, left and center panels). This was true in every run (Figure 6), so it was not an issue related to preconditioning of the catalyst before use. The end points of such kinetic data provided estimates for the steady-state CO coverages on the catalysts in relative terms, referred to full surface saturation (that is, the maximum

https://doi.org/10.1021/acscatal.5c03164
ACS Catal. 2025, 15, 12281−12292

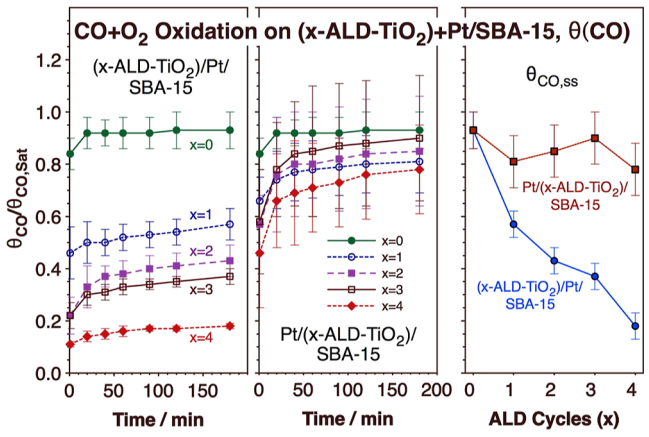

Figure 7. CO coverages on the surfaces of the Pt NP (relative to the maximum coverage measured under reaction conditions for Pt/SBA-15; $\theta_{CO}/\theta_{CO,sat}$) versus reaction time during the conversion of 100 Torr CO + 100 Torr O_2 gas mixtures at 425 K promoted by the (x-ALD-TiO_2)/Pt/SBA-15 (left panel) and Pt/(x-ALD-TiO_2)/SBA-15 (center) catalysts, both as a function of ALD cycles (x = 0 to 4). The data, extracted from the intensity of the peak at 2088 cm^{-1} in the in situ IR spectra in Figures 6, S4, and S5 (the last two in the Supporting Information), correspond to averages of the results from either five (for the (x-ALD-TiO_2)/Pt/SBA-15 catalysts) or two (Pt/(x-ALD-TiO_2)/SBA-15) individual runs. The steady-state $\theta_{CO}/\theta_{CO,sat}$ values are summarized versus x in the right panel.

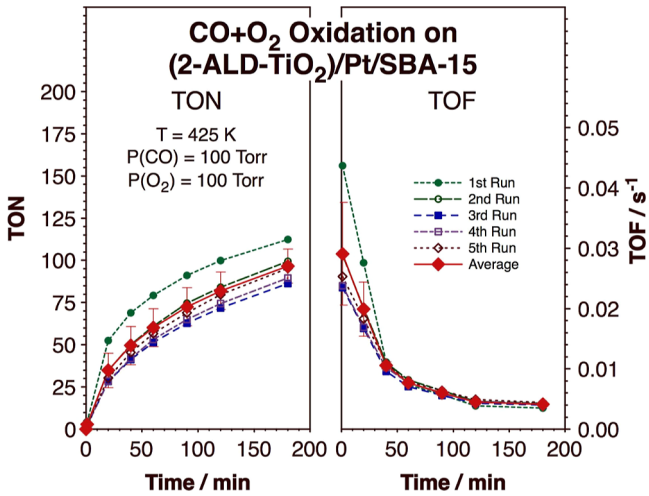

Figure 8. Kinetics of CO oxidation, in terms of TON (left panel) and TOF (right) versus time, for the conversion of 100 Torr CO + 100 Torr O_2 gas mixtures at 425 K promoted by the (2-ALD-TiO_2)/Pt/SBA-15 catalyst. Shown are the data from five consecutive reaction runs, extracted from the peak areas of the CO_2 peak in the in situ IR spectra shown in Figure 6, as well as the average values.

coverage seen under reaction conditions with the Pt/SBA-15 catalyst). A summary of those steady-state coverages is given for the two families of catalysts in the right panel of Figure 7. Relevant to our previous discussion on the CO titration experiments under vacuum is the fact that all Pt/(x-ALD-TiO_2)/SBA-15 catalysts display approximately the same coverage of Pt active sites, within experimental error, whereas in the (x-ALD-TiO_2)/Pt/SBA-15 cases, some Pt sites are clearly blocked by the TiO_2 deposited afterward. As already suggested above, the titania films appear to grow not only on the silica substrate but also on the Pt NPs if the ALD follows the Pt NP deposition. This effect is quite significant: by the fourth TiO_2 ALD cycle, as required to complete the first TiO_2 monolayer on the silica support, only about 20% of the initial Pt surface sites remain exposed.

The data for the kinetics of the CO conversion for all of the runs performed are reported in Figure S6 (Supporting Information), and an example of those, for the (2-ALD-TiO_2)/Pt/SBA-15 catalyst, is provided in Figure 8. Turnover numbers (TONs) were obtained by calibrating the IR CO_2 signal intensities (in independent experiments, filling the IR cell with varying pressures of CO_2) and dividing those by the total number of Pt surface atoms estimated by using the Pt loads and the average NP sizes reported for each catalyst in the center and right panels of Figure 2, respectively. Turnover frequencies (TOFs) were then calculated by numerical differentiation of the plots of TON versus time and are reported in units of s^{-1}.

The TON and TOF plots versus time obtained with all of the catalysts, averaged over all runs, are summarized in Figure 9. Also provided are the estimated initial and steady-state TOFs for both sets of catalysts as a function of the number of TiO_2 ALD cycles (x) used in their preparation (Figure 9, bottom-right panel). An increase in absolute TOFs with increasing x was observed in both cases for the catalysts prepared by adding the Pt NPs either before (data in blue) or after (red) the TiO_2 ALD, but the effect is more noticeable with the Pt/(x-ALD-TiO_2)/SBA-15 catalysts. However, that is because in the (x-ALD-TiO_2)/Pt/SBA-15 samples, there are fewer Pt sites exposed, as reported in Figure 7. If the TON and TOF values are normalized by the CO/Pt coverages estimated from the in situ IR measurements (Figure 7), then the trend reverses itself (Figure S7, Supporting Information). One interpretation of these results is that the Pt sites in the metal NPs modified by thin TiO_2 films may be intrinsically more active for the promotion of the oxidation of CO, but if so such a benefit is overcome by the fact that there are less active sites available overall, and on balance the catalysts made by growing the Pt NPs on top of the titania films perform better. However, the full picture is somewhat more complicated than that, as discussed later. A final point to be made here is that all these catalysts exhibit a relatively high activity at the start of the catalytic runs but the TOFs drop by about an order of magnitude within the first hour of reaction. This is not a reflection of catalyst poisoning or of major changes in their structure, however, because the initial rate is mostly regained once a fresh reaction mixture is fed into the reactor. Instead, it is possible that the product (CO_2) exerts an inhibiting effect on the reaction. This is an aspect of this reaction that is worth exploring further.

4. DISCUSSION

As stated in the Introduction, our main objective in this project has been to create, characterize, and optimize metal/reducible-oxide interface sites for the promotion of catalytic reactions, with a focus on oxidation processes. Our approach has relied on the growth of thin films of the oxides on mesoporous materials, SBA-15 in particular, because that provides a number of advantages, including: (1) the possibility of producing high-surface-area catalysts, something not always viable with the bulk materials of interests (titanium oxide in this case); (2) the ability to better control the growth of the films at a submonolayer level, and with that the structural and chemical properties of the resulting surfaces; and (3) the additional ability to better characterize the oxide surface sites

https://doi.org/10.1021/acscatal.5c03164
ACS Catal. 2025, 15, 12281−12292

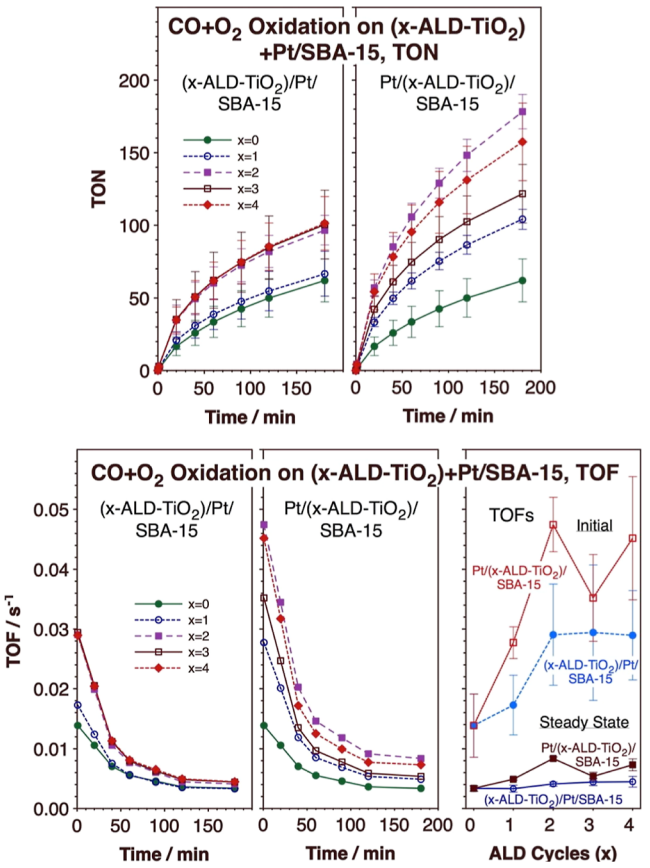

Figure 9. Kinetics of CO oxidation, in terms of TON (top row) and TOF (bottom) versus time, for the conversion of 100 Torr CO + 100 Torr O_2 gas mixtures at 425 K promoted by the (x-ALD-TiO_2)/Pt/SBA-15 (top left and bottom left, respectively) and Pt/(x-ALD-TiO_2)/SBA-15 (top right and bottom center) catalysts, both as a function of ALD cycles (x = 0 to 4). The data correspond to averages of the results from either five (for the (x-ALD-TiO_2)/Pt/SBA-15 catalysts) or two (Pt/(x-ALD-TiO_2)/SBA-15) individual runs (reported in Figure S6, Supporting Information). The initial and steady-state TOFs are summarized versus x in the bottom-right panel.

and distinguish them from the bulk material. Atomic layer deposition (ALD) was chosen as the way to build the oxide films because that process affords excellent conformality, even in porous materials, and control of the film thickness down to the submonolayer level. Such advantages were in fact corroborated in this work by the results from the isothermal N_2 adsorption−desorption measurements reported in Figures 1 and S1 (Supporting Information): the conformality was indicated by the retention of the narrow distribution of pore diameters seen in the initial SBA-15, and the rate of deposition by the extent to which that diameter decreases with increasing number of ALD cycles, at a linear rate of approximately 1.2 Å/cycle. The buildup of a full TiO_2 monolayer was reached by the fourth ALD cycle.

Pt NPs were added either before or after the growth of the titanium oxide films to create the desired metal/oxide interfaces. This provided an additional controllable parameter, which in fact proved to be critical for the chemical behavior of the catalysts, as discussed below. The average Pt NP sizes were approximately the same in all cases, somewhere between 4 and 6 nm in diameter, but smaller NPs were obtained when grown on the previously deposited TiO_2 film (Figures 2 and S2—Supporting Information). The structural details of the pores were nevertheless preserved in all cases (Figures 1 and S1—Supporting Information). Both the TiO_2 and Pt NP phases were well distributed throughout the length of the pores of the SBA-15 substrate (Figure 3). In this way, we were able to obtain a total of 9 samples with very similar structures but with TiO_2 films of different thicknesses (as the result of performing anywhere from 0 to 4 TiO_2 ALD cycles) and where the Pt NPs were added either before or after the oxide film growth.

The nature of the chemical sites in these catalysts was evaluated by using IR spectroscopy and CO as a probe molecule. In terms of the oxide surfaces, they could be titrated at cryogenic temperatures and the various sites identified by the associated C−O stretching frequencies of the adsorbed CO (Figure 4). It could be determined that the new sites added by the TiO_2 ALD were in fact different depending on the order of deposition with respect to the Pt NPs: when the titania films were grown first on the SBA-15, several CO adsorption sites were detected (in both cases, with or without Pt NPs), Lewis-acid fully coordinated Ti ions (Ti_{5C}) as well as possible mixed-oxide sites, but if the Pt NPs were added to the SBA-15 surface prior to the TiO_2 ALD, only one type of CO adsorption was detected, on the Ti sites.

It was also found that the interaction of the Pt NPs with the TiO_2 films affects the CO adsorption sites on the metal as well and that those are different depending on the order of the deposition of the two components. The relevant data are shown in Figures 5 and S3 (Supporting Information). The adsorption of CO on atop of Pt sites typically seen with Pt-based catalysts was observed in all of the catalysts studied here, but additional features were identified. If the TiO_2 films are grown on the SBA-15 support prior to the addition of the Pt NPs, a new CO IR peak develops identifiable with low-coordination sites. Those develop at the expense of the original atop sites, which are likely to be predominantly located in basal planes, possibly because the Pt NPs are smaller when grown on titania rather than silica surfaces (as mentioned above). Surprisingly, the new sites adsorb CO less strongly than the original atop sites, even if the former involve Pt atoms with lower coordination. More interesting are the catalysts in which the TiO_2 films are deposited on the Pt/SBA-15 solid. In that case, new low-frequency peaks are seen in the IR spectra that we contend reflect the adsorption of CO on Pt sites modified by TiO_2, possibly a thin layer grown on top of the metal NPs. The lower frequencies of the C−O stretching mode in the CO bonded to these sites suggest a higher degree of back-donation from the Pt d orbitals to the π^* antibonding orbital of CO and/or a more negatively charged Pt atom, the opposite to what has been reported for Au/TiO_2 catalysts.[32,49,50] It could be conceived that the new Pt sites become more electronegative upon interaction with the thin titanium film deposited on top. As a result, the CO bonding to the surface becomes stronger, and higher temperatures are required to induce its desorption.

The adsorption of CO on the Pt sites could also be probed by IR in situ during catalysis, while CO was being oxidized by O_2 (Figures 6 and 7, and S4 and S5—Supporting Information). The first observation worth pointing out here is that the only surface species detectable under reaction conditions is the CO bonded atop single Pt atoms; none of the other adsorption modes identified during the vacuum CO IR titration experiments were seen under the reaction conditions. This can be easily justified in terms of the energetics of the adsorption, since only the CO on atop sites survives heating

https://doi.org/10.1021/acscatal.5c03164
ACS Catal. 2025, 15, 12281−12292

the CO-dosed catalysts to 385 K under vacuum (Figure 5). Even the atop CO adsorbed species do not fully cover the Pt surface, and a dynamic adsorption−desorption equilibrium is established at the catalytic reaction temperature (425 K). By comparing the CO IR peak intensities in the titration (Figure 5) versus catalytic (Figures 6 and 7) experiments, we estimate that only roughly one-third to one-half of those sites are occupied during reaction on the Pt/(x-ALD-TiO_2)/SBA-15 (where the TiO_2 films were deposited before the Pt NPs). In the case of the (x-ALD-TiO_2)/Pt/SBA-15 counterparts (Pt NPs deposited first), fewer Pt atop sites are available to start with (because the TiO_2 films partially block the Pt NP surfaces), but still only about half of those are covered with CO at any time during catalysis. It is also worth noticing that reaching steady-state CO coverage under reaction conditions takes time, on the order of 1 h or so. It is possible that this is due to some reconstruction of the Pt NPs or the Pt/TiO_2 interfaces upon exposure to the CO + O_2 gas mixture at high temperatures. However, if this is so, the changes must be at least partially reversible, because subsequent catalytic runs reset the lower initial CO coverage and require similar times to again reach the steady state (Figure 7).

It is possible that even though no other CO adsorbed species besides that bonded atop individual Pt sites are detected by the in situ IR analysis of the catalysts during reaction, they may still participate in the CO oxidation process. We do not favor this possibility, however, because the intrinsic catalytic rates for CO oxidation measured here are similar in both sets of catalysts. As mentioned above, most of the unique CO adsorption sites observed in the IR data acquired at low temperatures (Figure 5) are depopulated under reaction conditions; they may possibly be relevant for other, milder catalytic processes but do not appear to contribute to the CO + O_2 conversion. Regardless, we speculate that at the very least, the Pt atop sites may provide a reservoir of CO-adsorbed species for reaction. In fact, the most accepted mechanistic model for this reaction with Au is the formation of a CO−O_2 complex at the Au/TiO_2 interface, even if that intermediate has not been directly detected during reaction (it was inferred from density functional theory—DFT—calculations).[55] Our own past in situ diffuse-reflectance IR (DRIFTS) experiments with Au/TiO_2 catalysts led to the identification of two CO-containing species on the surface, with peaks at 2180 and 2160 cm^{-1} assigned to adsorption on the titania surface and at the Au/TiO_2 interface, respectively, and to the observation of a correlation between the population of the second species and the catalytic activity.[38−40] Unfortunately, no equivalent feature could be seen in the in situ IR data from the experiments reported here, perhaps for a lack of sensitivity (the relevant IR peaks may be masked by the signal from gas-phase CO); a similar mechanism may nevertheless be operational with Pt as with Au.

In the same way as with the CO uptake, the rates of the CO oxidation also display a marked time evolution: the TOFs go down significantly, by about a factor of 5 or more, over a period of a couple of hours (Figure 9). Also like in the case of the buildup of the steady-state CO coverage on the Pt surface, the changes in TOF are mostly reversible, since they could be reset to their initial value upon pumping of the system and refilling of the reactor with a fresh reaction mixture. The first run of the CO + O_2 conversion with each catalyst did display a slightly higher reaction rate than that of all of the subsequent catalytic runs, but the difference amounted to an ∼25% change in the value, much less than the drops seen in each run versus time. On the other hand, the CO surface coverages during the reaction and the corresponding TOFs qualitatively follow similar trends; it would seem that the coverage of CO on Pt atop sites affects the rate of reaction. This correlation is not linear, however, since the temporal changes in TOFs are much more dramatic than those observed in the θ_{CO}'s. One possible interpretation of these results that is consistent with our other data is that the CO oxidation mechanism may occur at Pt/TiO_2 interface sites but requires prior CO adsorption on Pt and migration of those molecules from the atop Pt sites to the NP-border (Pt/oxide interface) sites.

In terms of the influence of the nature of the TiO_2 film on the kinetics of the CO oxidation reaction, it is clear from the data in Figure 9 that such films always enhance the catalytic activity. This is seen for films of various thicknesses, grown either before or after the deposition of the Pt NPs. However, the film thickness and the order of deposition are both critical in determining the catalyst relative performance. First, the TOFs increase in both cases, with both orders of TiO_2 + Pt NP deposition, in transitioning from no titania to 1 and 2 ALD cycles, after which they level off (within the accuracy of our experiments). The effect is more pronounced in the initial rates, but it is also seen under a steady state. In addition, higher rates are obtained if the Pt NPs are deposited on top of the pregrown TiO_2 films: the steady-state TOF with the Pt/(2-ALD-TiO_2)/SBA-15 catalyst is approximately twice that with the (2-ALD-TiO_2)/Pt/SBA-15 solid. It should be remembered, however, that in the latter case some of the Pt surface is covered by the titania film, about half for the case of 2 ALD TiO_2 cycles. In fact, normalized by the CO steady-state coverage, the reaction rates are comparable in both cases up to x = 2 (two ALD cycles) but diverge significantly (in the opposite direction) with thicker films, with the catalysts with the ALD carried out last becoming 2 to 3 times more active per exposed Pt atom (Figure S8—Supporting Information). It is worth adding that no evidence was obtained here for any significant amount of de-encapsulating of the Pt NPs, that is, of the removal of the TiO_2 overlayer deposited by ALD and partially covering the metal surface, during the CO + O_2 catalytic reaction, as it has been reported for Pt/TiO_2 catalysts during H_2 + O_2 conversions.[56]

The picture that emerges is one where CO is likely to first adsorb on the atop sites of the Pt NPs but then migrate to the Pt/TiO_2 interface for oxidation. The rate of the oxidation reaction is therefore controlled at least in part by the Pt surface area exposed. That area is reduced if the titania films are deposited on the Pt-containing catalysts, resulting in a decrease in the absolute reaction rate; the catalysts where the Pt NPs are deposited on the pregrown titania films are more active overall, even if that may not be the case in a per-exposed-Pt-atom basis. On the other hand, the catalysts with thicker TiO_2 films on top of the Pt/SBA-15 catalyst have metal/oxide interface sites that appear to be intrinsically more active than the regular sites in other catalysts. That may not necessarily reflect a change in the chemistry at the reaction site but may rather be due to the fact that as the titania films cover the Pt surface, they leave fewer metal sites unexposed but create more Pt/TiO_2 interface sites closer to the pure metal ones. In other words, there may be a CO diffusion term, from the initial Pt atop sites to the Pt/TiO_2 interface sites, that contributes to the overall kinetics of the CO oxidation reaction. Alternatively, there may be a higher surface density of Pt/TiO_2 sites overall to promote the CO

https://doi.org/10.1021/acscatal.5c03164
ACS Catal. 2025, 15, 12281−12292

oxidation step (once the CO molecules diffuse from the Pt sites) when the titania has been partially deposited on the surface of the metal NPs. On balance, it is clear that the addition of TiO_2 films enhances the performance of Pt-based catalysts in catalytic oxidation reactions but that there does not seem to be any advantage in adding the titania films on top of the Pt NPs; the best catalysts are those where the Pt NPs were deposited on the titania films instead. What is also clear is that a thin film of TiO_2, perhaps below a full monolayer coverage, is sufficient to confer the desirable properties via the creation of the metal/oxide interface sites that promote the oxidation reactions. This is good news, because depositing titania films on silica mesoporous materials rather than using pure titania solids affords catalysts with high surface areas. The optimization of the surface density of metal/oxide interface sites may then be achieved by controlling the size, shape, and dispersion of the metal NPs.

5. CONCLUSIONS

The use of ALD as a way to develop new catalysts comprising thin films of reducible oxides, TiO_2 in our study, was successfully probed, in this case to design Pt-based catalysts for the promotion of oxidation reactions (with CO). The films were shown to grow uniformly and conformally all throughout the length of the pores of a silica mesoporous material (SBA-15), with a thickness that could be controlled to a submonolayer level by choosing the appropriate number of ALD cycles. The structural characteristics of all catalysts were similar, except perhaps for the fact that the Pt NPs deposited on the titania films grew to slightly smaller average diameters. However, it was found that the order of the deposition between the oxide films and the metal NPs makes a big difference in the chemical reactivity of the catalysts. If Pt is deposited on the pregrown titania films, the metal NPs may be smaller and may expose different facets but otherwise behave similarly than when dispersed on the silica substrate. If titania is deposited on silica surfaces already containing Pt NPs, on the other hand, the metal surface becomes partially covered, and new Pt/TiO_2 interface sites are created, where CO adsorbs more weakly and displays lower C−O stretching frequencies.

On the basis of results from in situ IR characterization and kinetic experiments, CO oxidation on these catalysts was speculated to proceed via the initial adsorption of CO on Pt atop sites followed by migration to Pt/TiO_2 interface sites where the oxidation to CO_2 takes place. The presence of the TiO_2 film clearly enhances catalytic activity, but the nature of the new Pt/TiO_2 interface sites is likely to be similar in all catalysts, even before a full monolayer of TiO_2 is deposited. What changes is the number of Pt sites for CO adsorption and of Pt/TiO_2 interface sites for CO oxidation, and those yield maximum reaction rates if the TiO_2 is deposited first and at least 2 TiO_2 ALD cycles are used. Our general conclusions are likely to also apply to other oxidation reactions, even though previous results with Au instead of Pt showed some subtle differences.[31,32]

■ ASSOCIATED CONTENT

Supporting Information

The Supporting Information is available free of charge at https://pubs.acs.org/doi/10.1021/acscatal.5c03164.

Pore size distributions; STEM images and Pt NP size distributions; IR spectra of CO adsorbed on (x-ALD-TiO_2) + Pt/SBA-15 vs T; IR spectra during CO + O_2 oxidation on (x-ALD-TiO_2)/Pt/SBA-15 and Pt/(x-ALD-TiO_2)/SBA-15; kinetics of CO + O_2 oxidation on (x-ALD-TiO_2)/Pt/SBA-15; and summary of kinetics of CO + O_2 oxidation on Pt + (x-ALD-TiO_2)/SBA-15 (PDF)

■ AUTHOR INFORMATION

Corresponding Author

Francisco Zaera − *Department of Chemistry and UCR Center for Catalysis, University of California, Riverside, California 92521, United States;* orcid.org/0000-0002-0128-7221; Email: zaera@ucr.edu

Authors

Wang Ke − *Department of Chemistry and UCR Center for Catalysis, University of California, Riverside, California 92521, United States*

Ilkeun Lee − *Department of Chemistry and UCR Center for Catalysis, University of California, Riverside, California 92521, United States;* orcid.org/0000-0001-5718-7898

Complete contact information is available at: https://pubs.acs.org/10.1021/acscatal.5c03164

Notes

The authors declare no competing financial interest.

■ ACKNOWLEDGMENTS

Financial support for this project was provided by a grant from the U.S. Department of Energy, Office of Science, Basic Energy Sciences, Chemical Transformations Division, Catalysis Science Program, under award no. DE-SC0023119.

■ REFERENCES

(1) Doornkamp, C.; Ponec, V. The Universal Character of the Mars and Van Krevelen Mechanism. *J. Mol. Catal. A: Chem.* **2000**, *162* (1), 19−32.

(2) Ross, J. R. H. Chapter 7-the Kinetics and Mechanisms of Catalytic Reactions. In *Contemporary Catalysis*; Ross, J. R. H., Ed.; Elsevier, 2019; pp 161−186.

(3) Zhang, J.; Shu, M.; Niu, Y.; Yi, L.; Yi, H.; Zhou, Y.; Zhao, S.; Tang, X.; Gao, F. Advances in CO Catalytic Oxidation on Typical Noble Metal Catalysts: Mechanism, Performance and Optimization. *Chem. Eng. J.* **2024**, *495*, 153523.

(4) Chen, M. S.; Goodman, D. W. The Structure of Catalytically Active Gold on Titania. *Science* **2004**, *306* (5694), 252.

(5) Widmann, D.; Liu, Y.; Schüth, F.; Behm, R. J. Support Effects in the Au-Catalyzed CO Oxidation - Correlation between Activity, Oxygen Storage Capacity, and Support Reducibility. *J. Catal.* **2010**, *276* (2), 292−305.

(6) Liu, X. Y.; Wang, A.; Zhang, T.; Mou, C.-Y. Catalysis by Gold: New Insights into the Support Effect. *Nano Today* **2013**, *8* (4), 403−416.

(7) Yu, L.; Liu, Y.; Yang, F.; Evans, J.; Rodriguez, J. A.; Liu, P. CO Oxidation on Gold-Supported Iron Oxides: New Insights into Strong Oxide−Metal Interactions. *J. Phys. Chem. C* **2015**, *119* (29), 16614−16622.

(8) Ishida, T.; Murayama, T.; Taketoshi, A.; Haruta, M. Importance of Size and Contact Structure of Gold Nanoparticles for the Genesis of Unique Catalytic Processes. *Chem. Rev.* **2020**, *120* (2), 464−525.

(9) Ferraz, C. P.; Navarro-Jae'n, S.; Rossi, L. M.; Dumeignil, F.; Ghazzal, M. N.; Wojcieszak, R. Enhancing the Activity of Gold Supported Catalysts by Oxide Coating: Towards Efficient Oxidations. *Green Chem.* **2021**, *23* (21), 8453−8457.

(10) Thang, H. V.; Pacchioni, G. CO Oxidation Promoted by a Pt_4/TiO_2 Catalyst: Role of Lattice Oxygen at the Metal/Oxide Interface. *Catal. Lett.* **2019**, *149* (2), 390−398.
(11) Yoo, M.; Yu, Y.-S.; Ha, H.; Lee, S.; Choi, J.-S.; Oh, S.; Kang, E.; Choi, H.; An, H.; Lee, K.-S.; et al. A Tailored Oxide Interface Creates Dense Pt Single-Atom Catalysts with High Catalytic Activity. *Energy Environ. Sci.* **2020**, *13* (4), 1231−1239.
(12) Taleblou, M.; Camellone, M. F.; Fabris, S.; Piccinin, S. CO Oxidation over Platinum Nanoclusters: Unraveling the Role of the Cluster Size and the Supporting Surface. *J. Phys. Chem. C* **2023**, *127* (43), 21132−21149.
(13) Han, G.; Song, H. C.; Kim, S. H.; Park, J. Y. Role of the Support Oxidation State on the Catalytic Activity of Two-Dimensional Pt/TiO_x Catalysts. *J. Phys. Chem. C* **2023**, *127* (8), 4096−4103.
(14) Zhang, T.; Zheng, P.; Gao, J.; Liu, X.; Ji, Y.; Tian, J.; Zou, Y.; Sun, Z.; Hu, Q.; Chen, G.; et al. Simultaneously Activating Molecular Oxygen and Surface Lattice Oxygen on Pt/TiO_2 for Low-Temperature CO Oxidation. *Nat. Commun.* **2024**, *15* (1), 6827.
(15) Ruiz Puigdollers, A.; Schlexer, P.; Tosoni, S.; Pacchioni, G. Increasing Oxide Reducibility: The Role of Metal/Oxide Interfaces in the Formation of Oxygen Vacancies. *ACS Catal.* **2017**, *7* (10), 6493−6513.
(16) van Deelen, T. W.; Herna'ndez Meji'a, C.; de Jong, K. P. Control of Metal-Support Interactions in Heterogeneous Catalysts to Enhance Activity and Selectivity. *Nat. Catal.* **2019**, *2* (11), 955−970.
(17) Idriss, H. Oxygen Vacancies Role in Thermally Driven and Photon Driven Catalytic Reactions. *Chem Catal.* **2022**, *2* (7), 1549−1560.
(18) George, S. M. Atomic Layer Deposition: An Overview. *Chem. Rev.* **2010**, *110* (1), 111−131.
(19) O'Neill, B. J.; Jackson, D. H. K.; Lee, J.; Canlas, C.; Stair, P. C.; Marshall, C. L.; Elam, J. W.; Kuech, T. F.; Dumesic, J. A.; Huber, G. W. Catalyst Design with Atomic Layer Deposition. *ACS Catal.* **2015**, *5* (3), 1804−1825.
(20) Cao, L.; Lu, J. Atomic-Scale Engineering of Metal−Oxide Interfaces for Advanced Catalysis Using Atomic Layer Deposition. *Catal. Sci. Technol.* **2020**, *10* (9), 2695−2710.
(21) Plutnar, J.; Pumera, M. Applications of Atomic Layer Deposition in Design of Systems for Energy Conversion. *Small* **2021**, *17* (39), 2102088.
(22) Cho, Y.; D'Acunto, G.; Nanda, J.; Bent, S. F. Atomic and Molecular Layer Deposition on Unconventional Substrates: Challenges and Perspectives from Energy Applications. *Nanotechnology* **2025**, *36* (18), 182002.
(23) Zhao, D.; Feng, J.; Huo, Q.; Melosh, N.; Fredrickson, G. H.; Chmelka, B. F.; Stucky, G. D. Triblock Copolymer Syntheses of Mesoporous Silica with Periodic 50 to 300 Angstrom Pores. *Science* **1998**, *279* (5350), 548−552.
(24) Rahmat, N.; Abdullah, A. Z.; Mohamed, A. R. A Review: Mesoporous Santa Barbara Amorphous-15, Types, Synthesis and Its Applications Towards Biorefinery Production. *Am. J. Appl. Sci.* **2010**, *7* (12), 1579−1586.
(25) Singh, S.; Kumar, R.; Setiabudi, H. D.; Nanda, S.; Vo, D.-V. N. Advanced Synthesis Strategies of Mesoporous SBA-15 Supported Catalysts for Catalytic Reforming Applications: A State-of-the-Art Review. *Appl. Catal., A* **2018**, *559*, 57−74.
(26) Weng, Z.; Chen, Z.-h.; Qin, X.; Zaera, F. Sub-Monolayer Control of the Growth of Oxide Films on Mesoporous Materials. *J. Mater. Chem. A* **2018**, *6* (36), 17548−17558.
(27) Ke, W.; Liu, Y.; Wang, X.; Qin, X.; Chen, L.; Palomino, R. M.; Simonovis, J. P.; Lee, I.; Waluyo, I.; Rodriguez, J. A.; Frenkel, A. I.; Liu, P.; Zaera, F. Nucleation and Initial Stages of Growth During the Atomic Layer Deposition of Titanium Oxide on Mesoporous Silica. *Nano Lett.* **2020**, *20* (9), 6884−6890.
(28) Ke, W.; Qin, X.; Palomino, R. M.; Simonovis, J. P.; Senanayake, S. D.; Rodriguez, J. A.; Zaera, F. Redox Properties of TiO_2 Thin Films Grown on Mesoporous Silica by Atomic Layer Deposition. *J. Phys. Chem. Lett.* **2023**, *14*, 4696−4703.
(29) Zaera, F. New Advances in the Use of Infrared Absorption Spectroscopy for the Characterization of Heterogeneous Catalytic Reactions. *Chem. Soc. Rev.* **2014**, *43* (22), 7624−7663.
(30) Cao, Y.; Chen, B.; Guerrero-Sa'nchez, J.; Lee, I.; Zhou, X.; Takeuchi, N.; Zaera, F. Controlling Selectivity in Unsaturated Aldehyde Hydrogenation Using Single-Site Alloy Catalysts. *ACS Catal.* **2019**, *9*, 9150−9157.
(31) Qin, X.; Ke, W.; Vazquez, Y.; Lee, I.; Zaera, F. CO Oxidation Catalyzed by Au Dispersed on SBA-15 Modified with TiO_2 Films Grown via Atomic Layer Deposition (ALD). *Catalysts* **2023**, *13*, 1106.
(32) Ke, W.; Qin, X.; Vazquez, Y.; Lee, I.; Zaera, F. Direct Characterization of Interface Sites in Au/TiO_2 Catalysts Prepared Using Atomic Layer Deposition. *Chem Catal.* **2024**, *4*, 100977.
(33) Andersen, L. K.; Frei, H. Dynamics of CO in Mesoporous Silica Monitored by Time-Resolved Step-Scan and Rapid-Scan FT-IR Spectroscopy. *J. Phys. Chem. B* **2006**, *110* (45), 22601−22607.
(34) Shigeishi, R. A.; King, D. A. Chemisorption of Carbon Monoxide on Platinum {111}: Reflection-Absorption Infrared Spectroscopy. *Surf. Sci.* **1976**, *58*, 379.
(35) Sheppard, N.; Nguyen, T. T. Chapter 2: The Vibrationa Spectra of Carbon Monoxide Chemisorbed on the Surfaces of Metal Catalysts - A Suggested Scheme of Interpretation. *Adv. Infrared Raman Spectrosc.* **1978**, *5*, 67−148.
(36) Zaera, F.; Liu, J.; Xu, M. Isothermal Study of the Kinetics of Carbon Monoxide Oxidation on Pt(111): Rate Dependence on Surface Coverages. *J. Chem. Phys.* **1997**, *106* (10), 4204−4215.
(37) Wang, Y.; Woll, C. IR Spectroscopic Investigations of Chemical and Photochemical Reactions on Metal Oxides: Bridging the Materials Gap. *Chem. Soc. Rev.* **2017**, *46* (7), 1875−1932.
(38) Lee, I.; Zaera, F. Catalytic Oxidation of Carbon Monoxide at Cryogenic Temperatures. *J. Catal.* **2014**, *319*, 155−162.
(39) Lee, I.; Joo, J. B.; Yin, Y.; Zaera, F. Au@Void@TiO_2 Yolk−Shell Nanostructures as Catalysts for the Promotion of Oxidation Reactions at Cryogenic Temperatures. *Surf. Sci.* **2016**, *648*, 150−155.
(40) Lee, I.; Zaera, F. Effect of Metal Nanoparticle Size and Titania Crystallinity on the Performance of Au/TiO_2 Catalysts for the Promotion of Carbon Monoxide Oxidation at Cryogenic Temperatures. *J. Chem. Phys.* **2019**, *151* (5), 054701.
(41) Petrik, N. G.; Kimmel, G. A. Adsorption Geometry of CO Versus Coverage on TiO_2(110) from S- and p-Polarized Infrared Spectroscopy. *J. Phys. Chem. Lett.* **2012**, *3* (23), 3425−3430.
(42) Bradshaw, A. M.; Hoffmann, F. M. The Chemisorption of Carbon Monoxide on Palladium Single Crystal Surfaces: IR Spectroscopic Evidence for Localised Site Adsorption. *Surf. Sci.* **1978**, *72* (3), 513−535.
(43) Tauster, S. J.; Fung, S. C.; Garten, R. L. Strong Metal-Support Interactions. Group 8 Noble Metals Supported on Titanium Dioxide. *J. Am. Chem. Soc.* **1978**, *100* (1), 170−175.
(44) Fu, Q.; Wagner, T. Interaction of Nanostructured Metal Overlayers with Oxide Surfaces. *Surf. Sci. Rep.* **2007**, *62* (11), 431−498.
(45) Han, B.; Guo, Y.; Huang, Y.; Xi, W.; Xu, J.; Luo, J.; Qi, H.; Ren, Y.; Liu, X.; Qiao, B.; Zhang, T. Strong Metal−Support Interactions between Pt Single Atoms and TiO_2. *Angew. Chem., Int. Ed.* **2020**, *59* (29), 11824−11829.
(46) Monai, M.; Jenkinson, K.; Melcherts, A. E. M.; Louwen, J. N.; Irmak, E. A.; Van Aert, S.; Altantzis, T.; Vogt, C.; van der Stam, W.; Duchoň, T.; Šmíd, B.; Groeneveld, E.; Berben, P.; Bals, S.; Weckhuysen, B. M. Restructuring of Titanium Oxide Overlayers over Nickel Nanoparticles During Catalysis. *Science* **2023**, *380* (6645), 644−651.
(47) Xu, M.; Peng, M.; Tang, H.; Zhou, W.; Qiao, B.; Ma, D. Renaissance of Strong Metal−Support Interactions. *J. Am. Chem. Soc.* **2024**, *146* (4), 2290−2307.
(48) Ivanova, E.; Mihaylov, M.; Thibault-Starzyk, F.; Daturi, M.; Hadjiivanov, K. FTIR Spectroscopy Study of CO and NO Adsorption and Co-Adsorption on Pt/TiO_2. *J. Mol. Catal. A: Chem.* **2007**, *274* (1), 179−184.

https://doi.org/10.1021/acscatal.5c03164
ACS Catal. 2025, 15, 12281−12292

(49) Magkoev, T. T.; Rosenthal, D.; Schröder, S. L. M.; Christmann, K. Effect of the Titanium Oxide Stoichiometry on the Efficiency of CO Oxidation on the Au/TiO_x System Surface. *Tech. Phys. Lett.* **2000**, *26* (10), 894−896.
(50) Boccuzzi, F.; Chiorino, A.; Manzoli, M. Au/TiO_2 Nanostructured Catalyst: Pressure and Temperature Effects on the FTIR Spectra of CO Adsorbed at 90 K. *Surf. Sci.* **2002**, *502*−*503*, 513−518.
(51) Mikita, K.; Nakamura, M.; Hoshi, N. In Situ Infrared Reflection Absorption Spectroscopy of Carbon Monoxide Adsorbed on Pt(S)-[n(100)×(110)] Electrodes. *Langmuir* **2007**, *23* (17), 9092−9097.
(52) Lentz, C.; Jand, S. P.; Melke, J.; Roth, C.; Kaghazchi, P. Drifts Study of CO Adsorption on Pt Nanoparticles Supported by DFT Calculations. *J. Mol. Catal. A: Chem.* **2017**, *426*, 1−9.
(53) Ren, X.; Gobrogge, E. A.; Lundgren, C. A. Titrating Pt Surface with CO Molecules. *J. Phys. Chem. Lett.* **2019**, *10* (20), 6306−6315.
(54) Hossain, M. J.; Rahman, M. M.; Jafar Sharif, M. Preference for Low-Coordination Sites by Adsorbed CO on Small Platinum Nanoparticles. *Nanoscale Adv.* **2020**, *2* (3), 1245−1252.
(55) Green, I. X.; Tang, W.; Neurock, M.; Yates Jr, J. T. Spectroscopic Observation of Dual Catalytic Sites During Oxidation of CO on a Au/TiO_2 Catalyst. *Science* **2011**, *333* (6043), 736−739.
(56) Frey, H.; Beck, A.; Huang, X.; van Bokhoven, J. A.; Willinger, M. G. Dynamic Interplay between Metal Nanoparticles and Oxide Support under Redox Conditions. *Science* **2022**, *376* (6596), 982−987.

https://doi.org/10.1021/acscatal.5c03164
ACS Catal. 2025, 15, 12281−12292